ACS APPLIED MATERIALS & INTERFACES

Research Article

www.acsami.org

Space Survivable Polyimides with Excellent Optical Transparency and Self-Healing Properties Derived from Hyperbranched Polysiloxane

Xing F. Lei, Ying Chen, He P. Zhang, Xiang J. Li, Pan Yao, and Qiu Y. Zhang*

Department of Applied Chemistry, School of Science, Northwestern Polytechnical University, Youyi Road 127, Xi'an 710072, China

ABSTRACT: A novel space survivable polyimide with a variety of desirable properties such as excellent thermal stability, high optical transparency, good mechanical strength, satisfactory break elongation, and outstanding atomic oxygen (AO) erosion resistance has been prepared by first synthesizing hyperbranched polysiloxane (HBPSi) and second incorporating HBPSi into polyimide (PI) chains via copolycondensation reactions. The ^{29}Si nuclear magnetic resonance (^{29}Si NMR) spectrum of HBPSi indicated that HBPSi possessed hyperbranched topology. The ground-based simulated AO exposure experiments demonstrated the mass loss of HBPSi polyimides decreased with increasing HBPSi addition and AO fluence, and it reached as low as 7.7% that of pristine polyimide when HBPSi addition was 29.7 wt % after 22 h AO exposure. Surface morphologies confirmed that pristine polyimide was significantly roughened after AO exposure while HBPSi polyimide had even less rough surface topography. During exposure of HBPSi polyimide to AO, the organic polyimide of the surface was first degraded and a silica protective layer eventually formed, which enabled the surface to be "self-healing". It is this passivation layer that prevents the underlying polymer from additional erosion. The whole preparation process of HBPSi polyimide is moderate, low-cost, environmentally friendly, and suitable for industrialized mass production, which contributes this novel material to a "drop-in" replacement for the widely used Kapton on spacecrafts functioning in space environment.

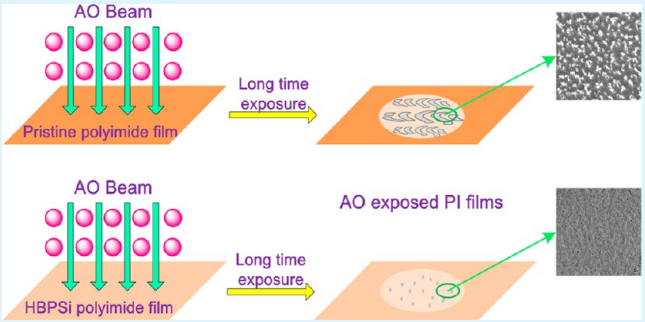

KEYWORDS: *low earth orbit (LEO), polyimide, atomic oxygen (AO), hyperbranched, polysiloxane*

1. INTRODUCTION

Organic materials, in particular Kapton and other polyimides, are ubiquitous on spacecrafts. Nevertheless, like all hydrocarbon-based polymers, polyimides are rapidly degraded in the highly oxidative environment of low earth orbit (LEO).[1−10] The primary mechanism for eroding organic hydrocarbon polymers is oxidation by atomic oxygen (AO), which can seriously reduce the service life of polymers and shorten the lifetime of the spacecrafts.[11−15] So far, extensive efforts have been made to prepare and fabricate anti-AO erosion materials that can be used to protect spacecrafts from rapid erosion by AO.[14−25]

Up to now, there are no commercially available polyimides inherently withstanding AO erosion. Commercially available polyimides that function in the LEO environment are generally protected from AO by a protective coating, such as aluminum, germanium, silica, or metallic oxides to prolong the service life.[17−20] Nevertheless, it is difficult to process a defect-free AO protective coating. Usually a specialized facility and a particular production procedure are required to manufacture such coatings. In addition, the shape and size of the film have been limited by the current coating technology. Moreover, difficulties in producing uniform coating and the mismatch of the coefficient of thermal expansion (CTE) between the substrate and the coating, as well as coating spalling, cracking, or disbonding are also thorny problems.[16] Furthermore, once damage occurs to the protective coating, the underlying polymer is again exposed to AO, and AO can attack and undercut the matrix through the sites of scratches, cracks, and erosion, which may lead to loss of mechanical and optical properties.[16−20] Therefore development of soft and AO resistant coatings with self-healing capabilities is desired.

In order to endow hydrocarbon-based polyimides with inherent anti-AO erosion properties, several promising methods including polymer blending,[25] copolymerization,[14−16] and organic−inorganic hybrid technology[26,27] have been developed during past several years. In this case, a new protective layer can be formed in situ on the topmost surface of polymer films to prevent the AO from eroding the underlying polymer materials.[16,26,27]

Fluorination is an alternative approach to reduce the AO erosion yield of polyimides. Many studies have reported a few fluorinated polyimides that exhibit desirable anti-AO erosion properties and function under the harsh conditions of the LEO environment. The groups of Tagawa and Minton[21−24] described fluorinated polyimide films spin-coated onto the

Received: July 22, 2013
Accepted: September 16, 2013
Published: September 16, 2013

electrode of a quartz crystal microbalance (QCM) and systematically studied the degradation behavior of fluorinated polyimide films. A relatively low AO erosion yield of 1.95×10^{-24} cm^3/atom was observed for fluorinated polyimide films. However, they also confirmed the certain role of extreme ultraviolet (EUV) radiation from the laser-sustained AO plasma in contributing to the erosion of a fluoropolymer under combined conditions, despite the fact that no strong synergistic effect or additive effect was observed even under the simultaneous exposure condition of AO and EUV/VUV. The above disadvantages, however, restricted the application of fluorinated polymers to be widely used in space because of ubiquitous extreme ultraviolet and vacuum ultraviolet (VUV) in LEO.

Phosphorus-containing polymers are another kind of attractive anti-AO erosion materials.[14−16,28−32] Upon vacuum AO exposure, a phosphorus oxide surface layer was formed on the surface of polymers, which effectively protected underlying polymers from additional erosion.[16,28] The India researchers have synthesized several kinds of phosphazene-based polymers and found that AO resistance was dependent on both the structure and phosphorus content of the polymer.[29] However, these materials exhibited relatively poor thermal performance. Another approach is to incorporate phenylphosphine oxide (PPO) groups into molecular backbones of polyimides by means of copolycondensation.[16,28,30−32] NASA researchers have prepared a novel diamine, [2,4-bis(3-aminophenoxy)-phenyl]-diphenylphosphine oxide, and subsequently reacted it with various dianhydrides to prepare PPO-containing polyimides.[16] Although the resulting polyimides exhibited high optical transparency, enhanced AO resistance, good tensile strength, and low solar absorptivity, these polyimide films were relatively brittle and exhibited poor fracture toughness. Moreover, polyimides containing PPO groups presented atomization phenomenon after long duration AO exposure.

Another method adopts silicon-containing components to form inorganic−organic polyimides, which can exhibit good mechanical properties as well as excellent thermal stability and outstanding durability when exposed to AO and UV to some extent.[26,27,33−36] Brunsvold et al.[26] revealed that the Si element in silicon-containing components got converted into a higher oxidation state in the form of SiO_2, which protected the underlying polymer from additional erosion. This is analogous to what has been reported to occur with phosphorus-containing polymers. Minton et al.[27] have prepared main-chain polyhedral oligomeric silsesquioxane (MC POSS) and incorporated MC POSS into the main chain of polyimide backbone by copolymerizing POSS monomers with the polyimide precursor. During exposure of POSS polyimide to an AO environment, organic material on the topmost surface was first degraded, and then a silica passivation layer was formed, which protected the underlying polymer from further degradation. However, during the synthesis of MC POSS, such expensive reagents as octacyclopentyl-POSS, *N*-*p*-lithiophenyl-*N*-1,1,4,4,-tetramethyl-disilylazacyclopentane, and *n*-BuLi were employed, and the preparation process was complicated and difficult to operate.[37] In order to reduce the production cost and simplify the experiment process, they have developed another side-chain POSS (SC POSS) polyimide. Nevertheless, the optical transparency, in particular that of the hybrid thin films after long duration AO exposure, which was crucial to solar absorptivity of polyimide films, was not taken into account in this research. Additionally, some costly reagents, such as (aminopropyl)-hepta-isobutyl-POSS, 3,5-dinitrobenzoyl chloride, and in particular platinum oxide, were used as well. Thus the whole development process of SC POSS polyimide was still relatively high-cost and adverse to commercial production.[27]

In summary, earlier studies generally focus on the durability of these special polyimides in LEO. The general performance, especially mechanical strength and optical transparency, is seldom measured quantitatively instead.[38,39] Furthermore, the whole development process is somewhat complex or high-cost. That is, the economic benefits are rarely taken into account. Based on the considerations listed above, development of low-cost novel polyimides with desirable general performance, such as high optical transparency, excellent inherent AO erosion resistance, perfect thermal stability, and good tensile strength is desired.

According to the anti-AO erosion mechanism of silicon-containing PIs, compounds with high silicon content and the structure with silicon of higher oxidation states are conducive to improving the AO resistance of PIs.[28] Recently, our group has designed and synthesized a series of hyperbranched polysiloxanes (HBPSi's) through a facile method, which has been used to prepare polymers with respect to particular properties or space applications. Analogously to POSS, HBPSi's possesses high silicon content and most of the silicons are in high oxidation states. Nevertheless, unlike the synthesis of POSS monomers, which was relatively high-cost, the synthesis of HBPSi only employed several kinds of low-cost siloxanes such as phenyltrimethoxysilane and γ-aminopropylmethyldiethoxysilane, and the whole preparation process was easy to operate and environmentally friendly. Moreover, several types of HBPSi's with different amino content or architectures could be easily obtained by controlling monomer addition manner and monomer molar ratio. Furthermore, more silicons can be incorporated into PI backbones without sacrificing other properties of PIs. HBPSi is a unique family of inorganic/organic hybrid three-dimensional compact structure that contains a silicon/oxygen network ($RSiO_n$, n = 1−2), where R is an organic group that can be utilized to tailor compatibility with the polymer or endows polymers with particular performance.[40] To the best of our knowledge, there has been no report yet about incorporating HBPSi into polyimide chains for the improvement of AO erosion resistance. In this paper, a new kind of space durable polyimide has been prepared through the incorporation of HBPSi into the molecular skeletons of Kapton-like polyimide via condensation polymerization of amination HBPSi monomers with the polyimide precursor. The AO erosion resistance of HBPSi polyimide has been investigated by exposing its surface to a variety of AO fluences. Additionally, the relationship between mass loss of polyimide films and AO fluence has been discussed. The changes of chemical components and structures of the film surface have also been examined. The surface morphologies of the AO-exposed films were observed using scanning electron microscopy (SEM). The optical transparency of the hybrid films before and after exposure to AO beams has also been measured. These evaluations may contribute to providing some effective insights into the degradation behavior and mechanism.

2. EXPERIMENTAL SECTION

2.1. Materials. γ-Aminopropylmethyldiethoxysilane (APMS) and phenyltrimethoxysilane (PTMS) were purchased from Nanjing Chengong Silicon Co., Ltd., and used as received. 4,4′-Diaminodiphenyl ether (ODA) and pyromellitic dianhydride (PMDA) were

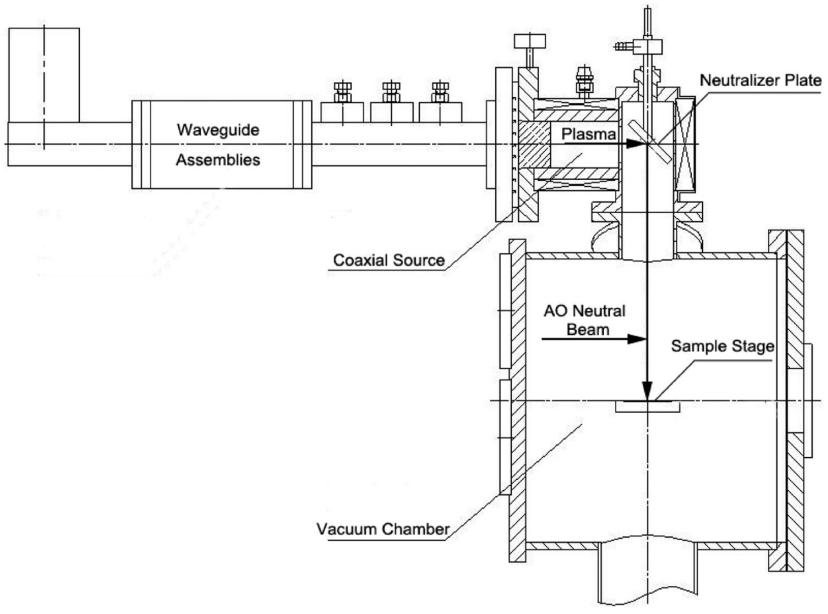

Figure 1. Cross-section view of low-energy neutral beam facility configured for beam energy measurements.

provided by Sinopharm Chemical Reagent Co. Ltd. and purified by vacuum sublimation prior to use. *N*,*N*′-Dimethylacetamide (DMAc) was purchased from Tianjin Fuyu Fine Chemicals Co. Ltd. and purified by distillation under reduced pressure over P_2O_5 prior to use.

2.2. Methods and Instruments. ^{29}Si nuclear magnetic resonance (NMR) measurement was acquired on a Bruker Avance 500 spectrometer (Bruker BioSpin, Switzerland) operating at 50.7 MHz in the solvent of $CDCl_3$. Chemical shift was referenced to tetramethylsilane (TMS). FT-IR spectrometer (BRUKER TENSOR 27) was employed to record the infrared spectra. The FT-IR spectrum of HBPSi was obtained by using thin KBr disk as the sample holder, while FT-IR spectra of polyimide films were collected by using an attenuated total reflectance (ATR) instrument. The molecular structure parameters of HBPSi were determined on a DAWN EOS size exclusion chromatography/multiangle laser light scattering (SEC/MALLS) instrument equipped with highly cross-linked styrene/divinylbenzene gel columns (500 Å, 5 μm) and a viscometer (Wyatt Technology). HPLC grade tetrahydrofuran (THF) was used as the eluent with a flow rate of 0.5 mL/min at 25 °C. Samples were first diluted with THF to a concentration of ca. 5 wt % and then filtered through a filter with a diameter of 0.22 μm. The molecular weight and the molecular weight distribution were determined by a SEC/DAWN EOS/Optilab rEX/QELS model. The intrinsic viscosity (η_n) and hydrodynamic radius ($R_{h(n)}$) were determined by a SEC/DAWN EOS/Optilab rEX/ViscoStar model, whereas the viscometer provided Mark−Houwink−Sakurada relationships. The refractive index increment (d*n*/d*c*) value of HBPSi was obtained by an Optilab rEX detector at 25 °C through a batch model. The ground-based simulated AO exposure experiments of pristine polyimide and HBPSi polyimide films were performed with an ECR-AB200 plasma atomic oxygen production instrument. The oxygen plasma was generated through the dissociation and ionizations of oxygen molecules by microwave produced by a microwave electron cyclotron resonance (ECR) oxygen neutral beam source operating at 3 kV and 55 mA. The cross-section view of the low-energy neutral beam facility is shown in Figure 1. The oxygen plasma mainly contains neutral O atoms, electrons, O_2^+, O^+, and molecular oxygen, with an ionic component of <0.1%. The mole fraction of atomic oxygen in the beam was above 90%. AO equivalent fluence measurements were calibrated based on 50 μm thick Kapton H film (DuPont, Inc.) mass loss, assuming an erosion yield of 3.0×10^{-24} cm^3·atom^{-1}.[9] The translational energy of AO was 3.0−10.0 eV. The neutral AO beam has a peak energy of ∼7 eV, with a full width at half-maximum (fwhm) in the distribution of ±3 eV. The AO flux is calculated from mass loss of Kapton H, by eq 1:[28,33]

$$f = \Delta m/(\rho AEt) \quad (1)$$

where f is the AO flux in the sample's position (atom·cm^{-2}·s^{-1}), Δm is the mass loss of Kapton H (g), ρ is the density of Kapton H (1.427 g/cm^3), A is the exposure area of Kapton H ($9\pi/4$ cm^2), E is the AO erosion yield of Kapton H (3.0×10^{-24} cm^3·atom^{-1}), and t is the exposure time (s) of Kapton H. In the current study, the AO flux at the sample's position was finally calibrated to be $\sim 4.89 \times 10^{15}$ atom·cm^{-2}·s^{-1}. The polyimide samples for measurement were small round pieces with diameters of 30 mm, which were subsequently dried in a vacuum oven at 80 °C for 4 h before AO exposure. During AO exposure, all samples were handled in a vacuum environment at ambient temperature, and the incoming AO attacked the polyimide film surface in a vertical direction. The mass loss was determined by using an analytical balance (HEG42-120200-7) with an accuracy of ±1 μg. All the exposed samples were handled in ambient air before surface analysis, including surface topography (SEM, AFM) and surface chemistry analysis (XPS). The film densities were measured by liquid suspension method. The surface morphologies of polyimide films before and after AO exposure were observed with a scanning electron microscope (SEM, JEOL JSM-6700F). Atomic force microscope (AFM) images and root-mean-square roughness values (RMS) of the resulting polyimide films before and after AO exposure were acquired using an SPI3800-SPA-400 (Japan, NSK Ltd.) scanning force microscope in tapping mode equipped with Olympus cantilevers (spring constant is 1.6 N/m) under ambient conditions. The elemental components and valence variations of the films before and after AO exposure were analyzed using a Thermo Scientific K-Alpha X-ray photoelectron spectroscopy (XPS) instrument. In the present work, the shifts of binding energy of XPS curves were corrected by assuming that the lowest C 1s component was 284.6 eV. The high-resolution XPS spectra of C 1s, Si 2p, and O 1s were curve-fitted according to XPS standard spectra databases and theoretical composition. The transmittance of the prepared films was measured by a U-3010 UV-vis spectrophotometer with the wavelength ranged from 200 to 800 nm. Thermal gravimetric analyses (TGA) of polyimide films were carried out with a Mettler Toledo TGA/DSC STARe apparatus at a heating rate of 10 °C/min under nitrogen atmosphere from room temperature to 1000 °C. Measurements of glass transition temperature of polyimide films were conducted using a Mettler Toledo DMA/SDTA861e instrument in tensile mode at a heating rate of 5 °C/min from room temperature to 420 °C. Tensile strength of self-standing polyimide films were measured using six specimens according to GB13022-91 at a drawing rate of 10 mm/min

Scheme 1. The Reaction Scheme for the Synthesis of HBPSi Monomer

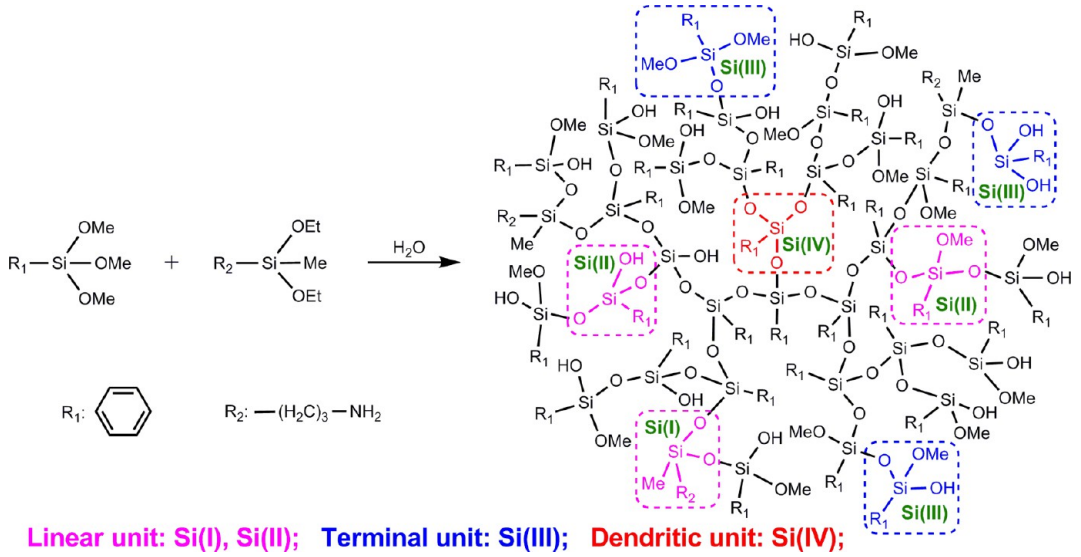

Table 1. Molecular Conformation Parameters of HBPSi from SEC

sample	M_n[a] (g/mol)	M_w[a] (g/mol)	M_w/M_n[a]	$R_{h(n)}$[a] (nm)	η_n[a] (mL/g)	α[a]	10^2K[a] (mL·g^{-1})	dn/dc[b] (mL/g)
HBPSi	3020	4045	1.34	0.4	1.0	0.41	6.85	0.136

[a]The macromolecular structure parameters were determined by SEC/MALLS equipped with a viscometer. [b]The refractive index increment (dn/dc) value of HBPSi was determined in THF by an Optilab rEX detector at 25 °C through a batch model.

at ambient temperature. Inherent viscosities of polyamic acid (PAA) were obtained on 0.5% (w/v) polyamic acid solutions in DMAc at 25 °C with an Ubbelohde viscometer.

2.3. Synthesis of HBPSi. Specifically, 1.2 g of APMS and 19.8 g of PTMS were mixed in a flask containing 22 g of distilled DMAc. Thereafter 4.6 g of deionized water was added dropwise over a period of 30 min to the mixture. Then the mixture was stirred in an ice−water bath for 1 h. Subsequently, the reaction system was stirred at 50 °C for another 2 h. Finally, the mixture was evaporated to remove alcohols, methanol, and water under a reduced pressure at 55 °C for about 2 h to give a transparent and viscous liquid with amino content of 0.46 mmol/g. The synthesis of HBPSi with a certain amount of amino groups and silanol groups is shown in Scheme 1.

2.4. Preparation of Pristine Polyimide (PMDA−ODA) and HBPSi Polyimide (PMDA−ODA/HBPSi) Thin Films. In current work, HBPSi was synthesized from APMS and PTMS. Therefore HBPSi was functionalized with a certain number of amino groups and could react with PMDA. Thus HBPSi polyamic acid (HBPSi PAA) could be easily acquired by copolymerizing reactions of amination HBPSi monomers, ODA, and PMDA in such polar aprotic solvents as DMAc, *N*,*N*′-dimethylformamide (DMF) or *N*-methylpyrrolidone (NMP). The detailed formulations for preparing pristine and HBPSi polyimides are listed in Table 1. The specific synthetic procedures were described as follows. First, HBPSi, ODA, or both were added into a flask and dissolved in DMAc with stirring under nitrogen atmosphere. After ODA had completely dissolved, equivalent PMDA was added and reacted at room temperature for 24 h with stirring under nitrogen atmosphere. The final content of polyamic acid (PAA) was 12 wt % in DMAc. Finally, the PAA solution was cast onto dust-free glass plates and put in an air-circulation oven soon afterward at 80 °C for 0.5 h. The imidization steps of these PAA was carried out by putting the samples in a temperature-programmable oven then heating to 360 °C at a heating rate of 4 °C min^{-1} and holding at 360 °C for 1 h. During the thermal imidization process, the HBPSi PAAs formed HBPSi polyimides through ring closure as well as concurrent loss of water. Thereafter the samples were allowed to cool to room temperature for at least 3 h to minimize the residual stress. At last, the glass plates were soaked in deionized water until the polyimide films could be peeled off. Subsequently, the films were dried in a vacuum oven at 120 °C for 4 h and then kept sealed for later testing. Scheme 2 gives the synthetic procedures for HBPSi polyimide thin films.

3. RESULTS AND DISCUSSION

3.1. Structure Analysis. *3.1.1. FT-IR of HBPSi.* Figure 2 depicted the FT-IR spectrum of HBPSi. The spectrum showed bands ascribed to phenyl groups, 1600 and 1440 cm^{-1} (C═C stretching) and 3058 and 3015 cm^{-1} (C−H stretching), and aminopropyl groups, 1500 cm^{-1} (N−H bending), 3420 cm^{-1} (N−H stretching), and 2860 and 2925 cm^{-1} (C−H stretching).[41,42] The intense absorption peak at 1135 cm^{-1} confirmed the presence of Si−O−Si network in HBPSi. The characteristic band at 3420 cm^{-1} (N−H stretching) suggested HBPSi has been functionalized with amino groups.

3.1.2. ^{29}Si NMR of HBPSi. The ^{29}Si NMR of HBPSi was presented in Figure 3. Figure 3 confirmed there existed four different silicon atoms in HBPSi. The four chemical shifts at −18.4, −71.5, −69.9, and −79.5 ppm were defined as Si(I), Si(II), Si(III), and Si(IV) units, respectively. Si(I) and Si(II) were assigned to linear units. Si(III) represented terminal units, and Si(IV) was ascribed to a dendritic unit.[43−46] The peak at −79.5 ppm was much more pronounced than the other three peaks, indicating that dendritic unit was ubiquitous in HBPSi and most of PTMS monomers were completely hydrolyzed and eventually in the form of RSi(OSi)$_3$ (R refers to the phenyl group). The degree of branching (DB) of HBPSi was thus estimated to be 0.95 and 0.91, which were determined based on the ^{29}Si NMR spectrum according to Frey's equation (eq 2)[47] and Fréchet's equation (eq 3),[48] respectively.

$$DB = 2D/(2D + L) \quad (2)$$

$$DB' = (D + T)/(D + T + L) \quad (3)$$

Scheme 2. The Reaction Scheme for the Synthesis of HBPSi Polyimide Thin Films

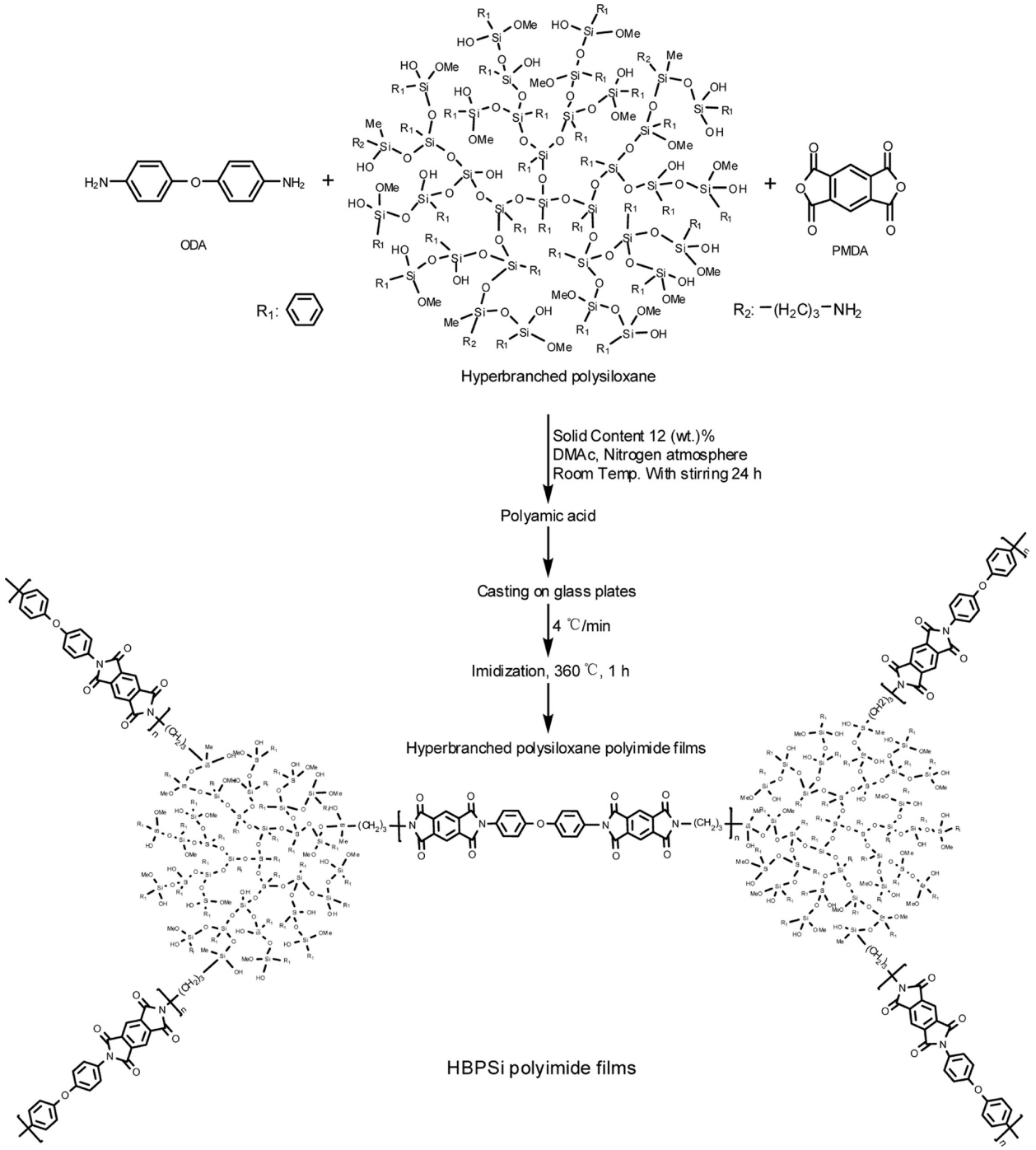

DB of HBPSi was close to 1 and significantly higher than that of the conventional hyperbranched polymers.[40,49−53] Thus HBPSi is likely to have "completely branched" structure. However, it should be noted that although most of the PTMS was completely hydrolyzed, HBPSi was still less perfect in structure than common dendrimers due to the random polymerization process as well as inevitable intramolecular cyclizations during the condensation reactions of silanols,[47] which might lead to an increase to DB.

3.1.3. Molecular Structure Analysis of HBPSi. The molecular structure parameters of HBPSi were investigated by SEC/MALLS equipped with a viscometer (Wyatt Technology). The specific results are shown in Figure 4 and Table 1. The M_w and molecular weight distribution of HBPSi were 4045 g/mol and 1.34, respectively. The hydrodynamic radius ($R_{h(n)}$) of HBPSi was 0.4 nm. In order to study the compact conformation of HBPSi, its intrinsic viscosity value, $[\eta]$, was measured in THF at 25 °C by SEC. The intrinsic viscosity of polymers is correlated with their molecular weight by the Mark−Houwink−Sakurada (MHS) equation:

$$[\eta] = KM^{\alpha} \quad (4)$$

where α, the MHS exponent, is a parameter corresponding to the topology of a polymer in a good solvent.[49,52,54] For hyperbranched polymers, the exponent typically varies from 0.5 to 0.2, depending on the degree of branching. In contrast, the

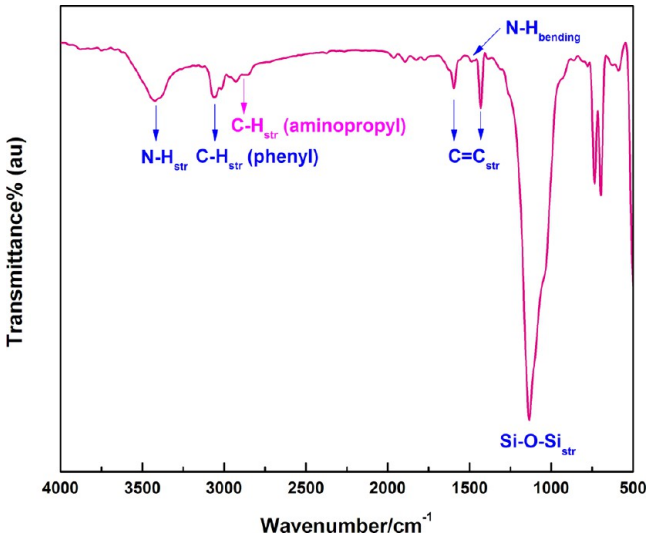

Figure 2. FT-IR spectrum of HBPSi.

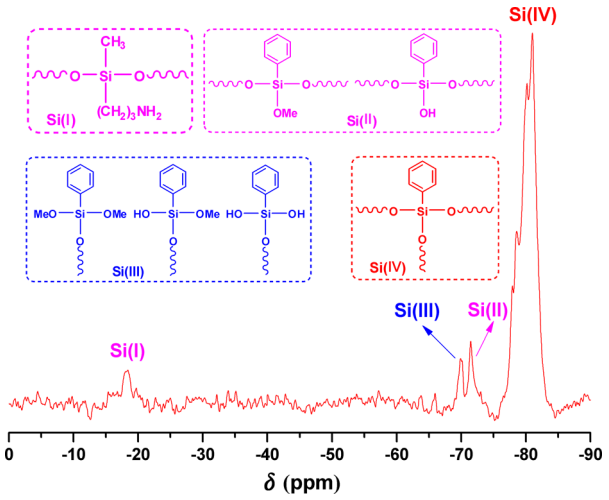

Figure 3. ^{29}Si NMR spectrum of HBPSi.

MHS exponent is typically in the range of 0.6−0.8 for a linear polymer in a good solvent with a random coil conformation.[49,52,54] The MHS exponent of HBPSi was 0.41, which was significantly lower than that of a linear polymer, further demonstrating HBPSi possessed highly branched architectures.

3.1.4. FT-IR Spectra of HBPSi-PI. The incorporation of HBPSi in the polyimides was demonstrated by FT-IR measurement. Figure 5 shows the FT-IR spectra of the pristine

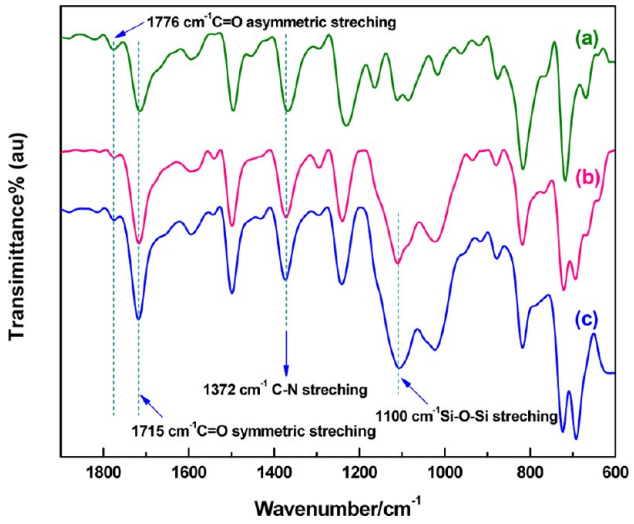

Figure 5. FT-IR spectra of (a) pristine polyimide, (b) 4.1 wt % HBPSi polyimide, and (c) 29.7 wt % HBPSi polyimide.

and HBPSi polyimides. The appearance of characteristic imide group peaks at 1776 cm^{-1} (C═O asymmetrical stretching), 1715 cm^{-1} (C═O symmetric stretching), 1372 cm^{-1} (C−N stretching), and 720 cm^{-1} (C═O bending) and the absence of the characteristic peaks of polyamic acid around 1650 cm^{-1} in FT-IR spectra suggested a complete conversion of all polyamic acid into the polyimides. The intense absorption at 1100 cm^{-1} (Si−O stretching) confirmed that Si−O−Si network was present in HBPSi polyimide hybrid films.[55,56]

3.2. Properties of the Prepared Polyimide Films. A few properties of the prepared polyimide films are presented in Table 2. The intrinsic viscosities of PAA ranged from 1.03 to 3.32 dL/g, indicating medium to high molecular weight polymer formation. The pristine polyamic acid exhibited the

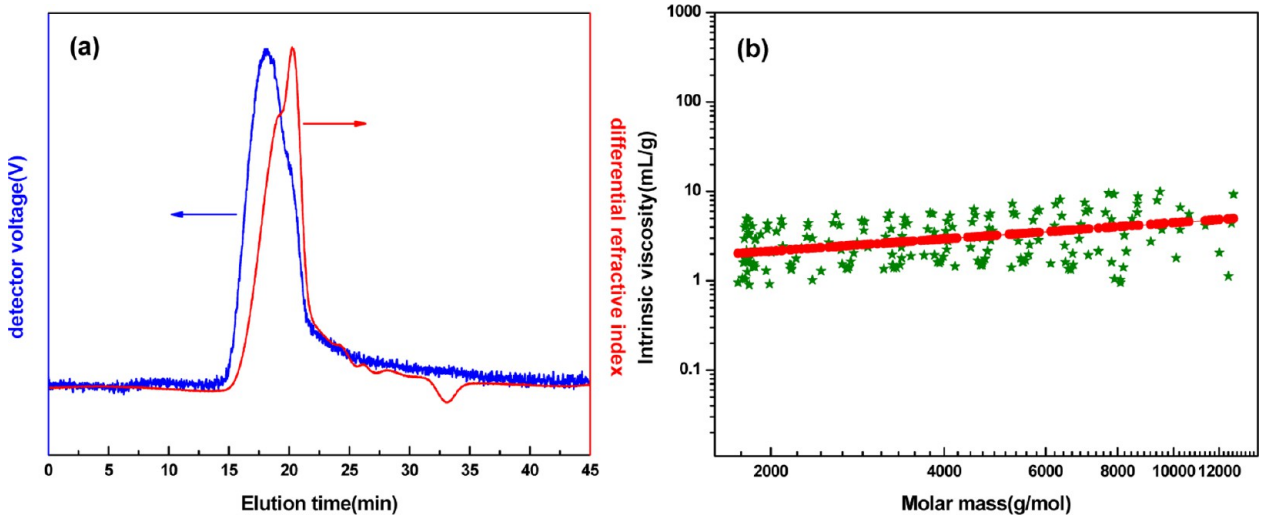

Figure 4. (a) MALLS-SEC elution curves of HBPSi; (b) Mark−Houwink−Sakurada plots of HBPSi.

Table 2. Recipe and Properties of Pristine and HBPSi Polyimide Thin Films

sample code[a]	ODA (g)	PMDA (g)	HBPSi (g)	DMAc (g)	wt % HBPSi in polyimide	intrinsic viscosities (dL/g)	film density(g·cm^{-3})	T_d[b] (°C)	T_g[c] (°C)	transparency at 600 nm (%)	tensile strength (MPa)	break elongation (%)
PI-0	2.00	2.18		30.65	0	3.32	1.39	571	371	79	113	26
PI-4.1	1.99	2.18	0.18	31.90	4.1	2.14	1.38	564	390	76	102	22
PI-8.8	1.98	2.18	0.40	33.44	8.8	1.42	1.36	569	376	75	98	21
PI-14.4	1.97	2.18	0.70	35.56	14.4	1.20	1.34	572	372	78	90	18
PI-21.9	1.95	2.18	1.16	38.79	21.9	1.12	1.32	574	376	76	87	16
PI-29.7	1.92	2.18	1.73	42.75	29.7	1.03	1.30	575	378	78	80	15

[a]PI-*x* represents polyimide sample, where "*x*" refers to the mass fraction of HBPSi in the resulting polyimide. For example, PI-0 means pristine polyimide and PI-29.7 represents 29.7 wt % HBPSi polyimide. [b]Thermal decomposition temperature at 5 wt % mass loss under nitrogen atmosphere. [c]Glass transition temperature.

highest intrinsic viscosity, whereas HBPSi-containing PAA presented decreased intrinsic viscosity with increasing HBPSi content, demonstrating that the incorporation of HBPSi probably affected the growth of the molecular weight. The 5 wt % thermal decomposition temperatures (T_d) and glass transition temperatures (T_g) of prepared films are shown in Table 2. The variance of T_d was possibly caused by molecular weight and benzene ring content. As the intrinsic viscosities show, the incorporation of HBPSi probably affected the growth of the molecular weight, which generally caused T_d to decrease while the factor of the increasing benzene ring content of HBPSi enhanced T_d . When the former effect surpassed that of the latter, T_d of polyimides when HBPSi loading amount were relatively low, such as 4.1 and 8.8 wt %, slightly decreased relative to that of pristine polyimide. Likewise, when the latter effect was dominant, T_d might gradually increase. Among all the prepared polyimide films, T_g reached the highest at 4.1 wt % HBPSi loading amount, but it was lowest at 14.4 wt %. As is known, T_g is possibly determined by the interaction of three factors, molecular weight, rigidity (or mobility) of molecular chains, and degree of cross-linking. As shown in Table 2, 4.1 wt % HBPSi polyamic acid exhibited the second highest intrinsic viscosity, indicating the highest molecular weight polymer formation among all the HBPSi polyimides, which was favorable to improve T_g. Meanwhile, the rigidity of polyimide chains was probably significantly enhanced owing to the HBPSi incorporation although the molecular weight slightly decreased, leading to higher T_g as well. In addition, the incorporation of HBPSi could possibly generate cross-linking effects, which was also responsible for higher T_g than that of pristine polyimide. Thus it would make sense that 4.1 wt % HBPSi polyimide exhibited highest T_g among all the resulting polyimides. For 14.4 wt % HBPSi polyimide, the molecular weight was lower than that of pristine polyimide and 4.1−8.8 wt % HBPSi polyimides. Additionally, the rigidity of molecular chains as well as degree of cross-linking was also lower than that of 21.9−29.7 wt % HBPSi polyimides due to lower HBPSi loading amount. The above three factors possibly result in the lowest T_g of 14.4 wt % HBPSi polyimide of all the HBPSi polyimides. As indicated, T_d and T_g of the resulting films were all above 560 and 370 °C, respectively, indicating excellent thermal stability. The typical thermal cycle experienced by spacecrafts in LEO is ±100 °C.[16] Thus, the thermal performances of these hybrids are sufficient for use in LEO. Figure 6 illustrates the TGA curves of the prepared polyimide films at a heating rate of 10 °C/min under nitrogen flow. As indicated, the increasing residues at 1000 °C from PI-0 to PI-29.7 also suggested the successful incorporation of the HBPSi moiety in the hybrid materials. All of the prepared films were flexible and foldable

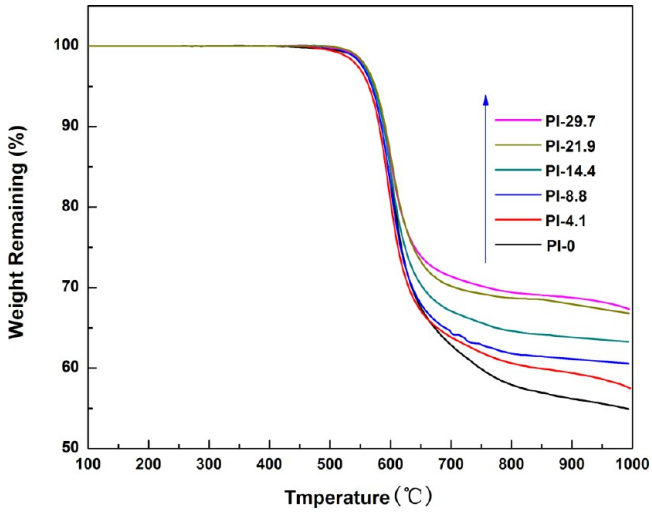

Figure 6. TGA curves of prepared films at a heating rate of 10 °C/min under nitrogen flow.

and displayed high optical transparency. The films exhibited tensile strength and break elongation from 80−113 MPa and 15−26%, respectively. The decreasing tensile strength and break elongation was possibly attributed to lower molecular weight and increasing stiffness of molecular chains. Moreover, the bulky spheroid structure and steric hindrance of HBPSi possibly increased the interval between polyimide chains, which resulted in the increase of free volume of the polyimide matrix and led to poor interactions between polymer chains, as further evidenced by the decreasing film densities shown in Table 2. In addition, HBPSi consists of a great many Si−O bonds, which were less polar than imide rings. As a result, the packing density and interactions between polymer chains were weakened as HBPSi addition increased.[57] To sum up, despite HBPSi having minor effects on the mechanical strength of the hybrid films, the tensile strength and break elongation were all above 80 MPa and 15%, respectively, which was tough enough for use in LEO, as compared with the reported results.[16]

The relative mass loss of HBPSi polyimide films to pristine polyimide film was shown in Figure 7. The mass loss of hybrid films decreased dramatically with increasing the HBPSi content. When HBPSi addition reached 29.7%, the hybrid films exhibited a weight loss of ∼17.5% that of pristine polyimide. According to eq 1, this was calculated to be an erosion yield of 5.38×10^{-25} cm^3/atom. More specifically, in an AO exposure with a total fluence of 3.87×10^{20} O atoms cm^{-2} (AO exposure for 22 h), the erosion yield was calculated to be 2.39×10^{-25} cm^3/atom, which was merely 7.97% that of standard Kapton H

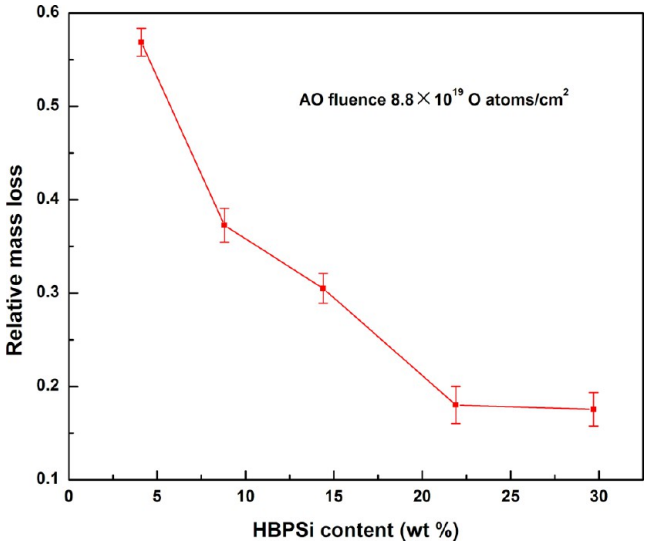

Figure 7. Relative mass loss of HBPSi polyimide films with different HBPSi content to pristine polyimide film after AO exposure for 5 h.

(3×10^{-24} cm^3/atom). However, as the earlier results reported,[27,58] the mass loss of pristine polyimide increased linearly with increasing total AO fluence due to the constant erosion yield (3×10^{-24} cm^3/atom), while the erosion yield of silicon-containing polyimide decreased exponentially with increasing AO fluence. Hence, in order to clarify the oxidation degradation mechanism and behavior of HBPSi polyimides, the mass loss was investigated at different AO exposure duration in the current study. As shown in Figure 8, the mass loss of

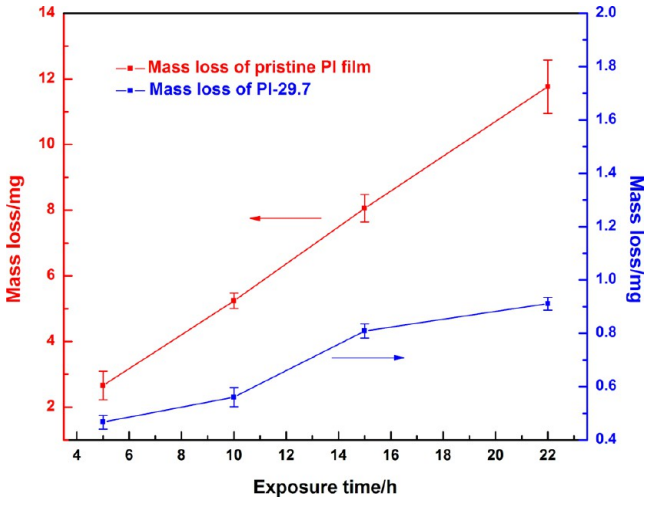

Figure 8. Mass loss of pristine polyimide and 29.7 wt % HBPSi polyimide at different AO exposure duration.

pristine polyimide approximately exhibited as a linear function of total AO fluence over the 22 h exposure period, while the mass loss of 29.7 wt % HBPSi polyimide exhibited a nonlinear mass loss but gradually increased as a power function ($y = x^a$, $a < 1$; considering that the data were not continuous and were insufficient, the specific function expression was not given) throughout the duration of the AO exposure.[36] From Figure 8, the decreasing relative mass loss at different AO exposure duration suggested that the HBPSi moiety had played an indispensible role in resistance to AO erosion. Specifically, after 22 h AO exposure (AO total fluence was 3.87×10^{20} O atoms·cm^{-2}), the mass loss of 29.7 wt % HBPSi polyimide merely reached 7.7% that of pristine polyimide.

3.3. Surface Morphologies of Polyimide Films. SEM and AFM images of pristine polyimide and 29.7 wt % HBPSi polyimide films before and after AO exposure are presented in Figures 9 and 10. Before AO exposure, as shown in Figure 9A,F, the sample surfaces were flat and smooth, in accordance with the small RMS values summarized in Table 3. However, the surface morphologies had significantly changed with increasing exposure fluence, in particular the pristine polyimide film surfaces. As shown in Table 3, Figure 9B–E, and Figure 10B–E, the pristine polyimide surfaces became increasing rough with increasing exposure fluence and exhibited "carpet-like" topography. After AO exposure, the surfaces of the pristine polyimide displayed numerous short cones and undulate patterns, and the short cones gradually became larger. Meanwhile, the RMS values rapidly increased with increasing AO fluence. After 22 h exposure, the RMS value was up to 327.6 nm, indicating that the pristine polyimide surface was significantly roughened after long duration AO exposure. The surfaces of 29.7 wt % HBPSi polyimide also became increasingly rough with increasing exposure fluence but to a much lower extent than the pristine polyimide surfaces. By contrast, the surfaces of 29.7 wt % HBPSi polyimide were smoother and denser except for the presence of a certain amount of pinholes and microcracks. It was obvious that the surfaces of hybrid films had shown more compact surface structure and outstanding AO erosion resistance. This was possibly because the incoming AO reacted indiscriminately with the topmost surface atoms, which were carbon, nitrogen, hydrogen, or silicon. Among these surface atoms, only silicon formed an oxide that was nonvolatile. Thus the polyimide portions on the topmost surface were etched and a silicon-rich layer gradually formed on the topmost surface, which possibly retarded additional erosion.[26,27,36,59] For pristine polyimide, the lack of a silicon-rich protective layer resulted in continuous oxidative degradation of the organic portions, namely, undercutting erosion, leading to dramatic mass loss and an extremely rough surface. It is worth noting that the pinholes and microcracks appearing on the hybrid film surface played a significant role in the mass loss of hybrid films during AO exposure and will be discussed later.

3.4. XPS Analysis. Pristine polyimide films and 29.7 wt % HBPSi polyimide films for different exposure periods were analyzed by XPS to characterize changes in oxidation states and compositions of the surface atoms. Table 3 illustrated the surface elemental compositions of pristine polyimide and 29.7 wt % HBPSi polyimide that were exposed to a variety of fluences (exposure periods). For the pristine polyimide surface, the carbon atom concentrations decreased insignificantly, while the oxygen atom concentrations increased somewhat with increasing exposure fluence. However, as can be seen from Table 3, the decrease in carbon atom concentration was much more dramatic for 29.7 wt % HBPSi polyimide surface. Similarly, the increase in oxygen atom concentration was much more remarkable for 29.7 wt % HBPSi polyimide than for pristine polyimide. The silicon atom concentration on the surface of unexposed hybrid polyimide was very low, only a few percent. Nevertheless, after AO exposure, the silicon atom concentrations dramatically increased and tended to a steady-state value as the exposure duration increased. In addition, the Si/O ratio tended approximately toward 1:2, suggesting

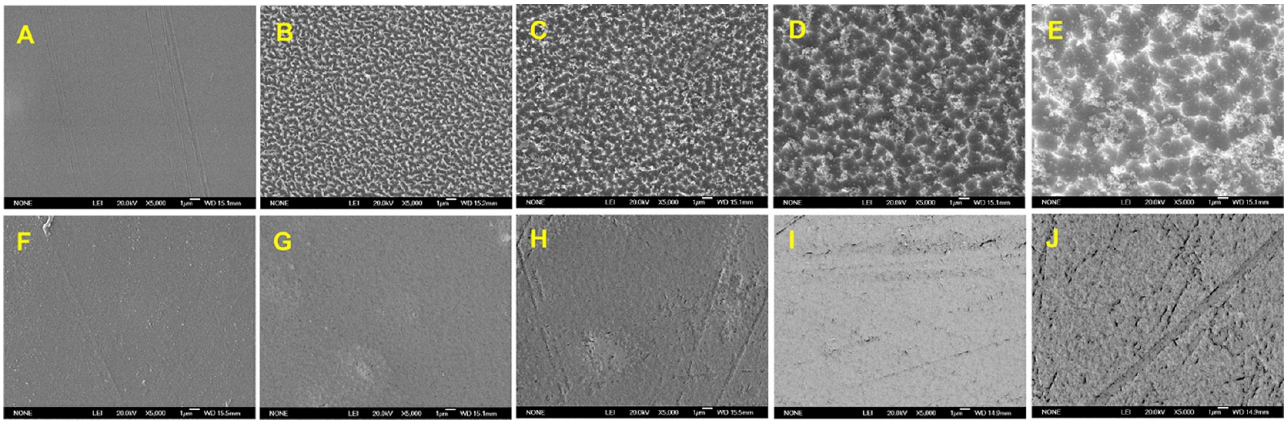

Figure 9. SEM images of pristine polyimide films (A–E) and 29.7 wt % HBPSi polyimide films (F–J) before and after exposure to a variety of AO fluences of 0.88×10^{20}, 1.76×10^{20}, 2.64×10^{20}, and 3.87×10^{20} O atoms·cm^{-2} respectively.

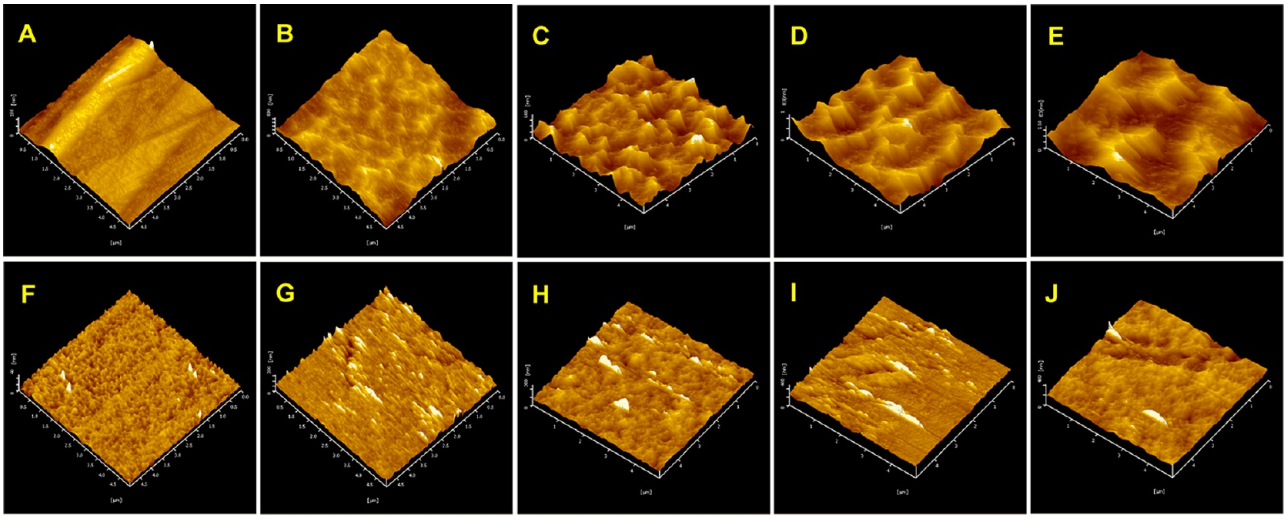

Figure 10. Three-dimensional AFM images (5 μm × 5 μm) of pristine polyimide films (A–E) and 29.7 wt % HBPSi polyimide films (F–J) before and after exposure to a variety of AO fluences of 0.88×10^{20} O, 1.76×10^{20}, 2.64×10^{20}, and 3.87×10^{20} O atoms·cm^{-2}.

Table 3. AO Erosion Data, Optical Transparency, and Root Mean Square Roughness Values (RMS) as Well as Surface Atomic Concentrations (atom %) Determined from XPS Survey Scans for Pristine Polyimide and 29.7 wt % HBPSi Polyimide before and after Exposure to a Variety of AO Fluences

					surface atomic concentrations (atom %)			
sample	Kapton-equivalent AO fluence ($\times 10^{20}$ O atoms·cm^{-2})	mass loss (mg)	transparency at 600 nm (%)	RMS (nm)	C 1s	N 1s	O 1s	Si 2p
pristine PI	0		79	2.66	76.6	6.8	16.6	0
	0.88	2.662 ± 0.435	72	111.7	69.8	11.7	18.5	0
	1.76	5.242 ± 0.235	36	126.5	65.9	14.9	19.2	0
	2.64	8.058 ± 0.422	22	195.2	64.0	16.2	19.8	0
	3.87	11.765 ± 0.812	18	327.6	62.5	17.2	20.3	0
29.7 wt % HBPSi-PI	0		78	3.17	71.4	4.8	17.9	5.9
	0.88	0.467 ± 0.026	76	13.27	12.4	4.5	54.7	28.4
	1.76	0.561 ± 0.036	76	22.61	9.9	5.7	55.4	29.0
	2.64	0.809 ± 0.026	72	25.3	8.5	4.6	58.1	28.8
	3.87	0.911 ± 0.024	62	28.4	7.1	0	63.8	29.1

possible formation of a silica layer on the topmost surface of 29.7 wt % HBPSi polyimide.

High-resolution XPS spectra of C 1s, Si 2p, and O 1s peaks corresponding to 29.7 wt % HBPSi polyimide exposed to a variety of fluences are given in Figure 11a–c, respectively. As shown in Figure 11a, the peaks at 284.6 eV (C–H or C–C), 286.4 eV (C–O, C–N), and 288.5 eV (C═O) became dramatically less pronounced after exposure to AO. As known to all, the imide ring (nitrogen element) and carbonyl group were characteristic chemical structures associated with poly-

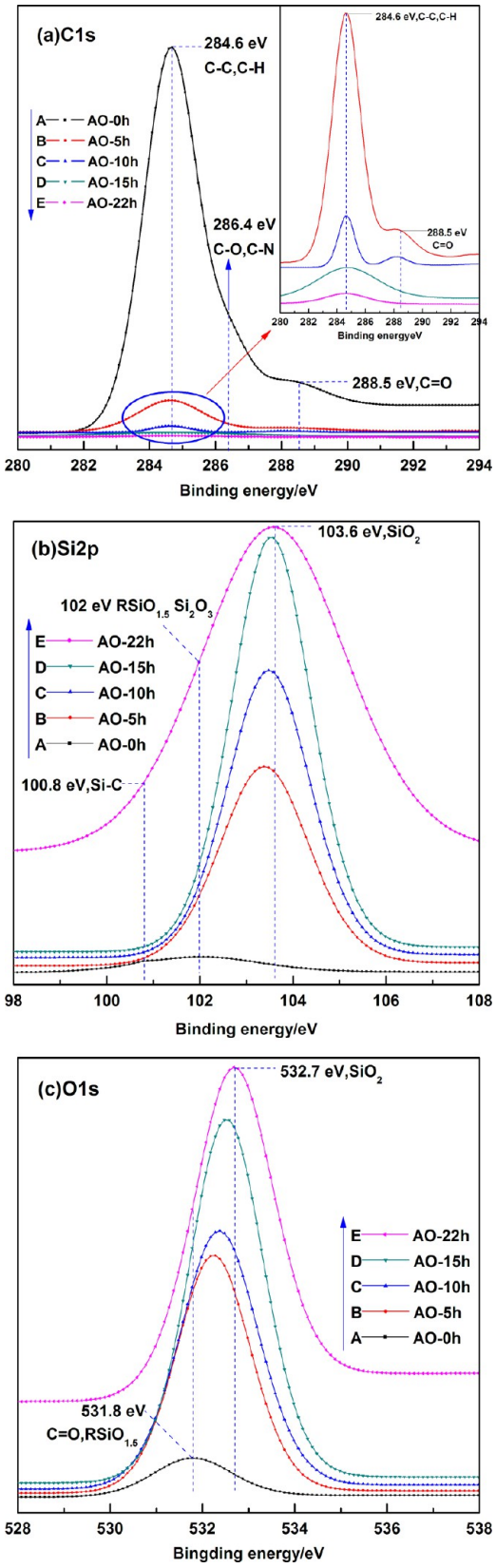

Figure 11. High-resolution XPS spectra of 29.7 (wt.)% HBPSi polyimide films: (a) C 1s, (b) Si 2p, and (c) O 1s before and after AO exposure with total AO fluence of 0.88×10^{20} O atoms·cm^{-2} (5 h), 1.76×10^{20} O atoms·cm^{-2} (10 h), 2.64×10^{20} O atoms·cm^{-2} (15 h), and 3.87×10^{20} O atoms·cm^{-2} (22 h).

imide. However, as the total AO fluence increased to 3.87×10^{20} O atoms·cm^{-2}, the signals of C−N and C═O were hardly detected, in agreement with the surface atom concentrations shown in Table 3. This is to say that the entire organic polyimide moiety on the topmost surface had almost been etched by the incoming AO. This was probably due to the oxidative degradation of carbon, hydrogen, or nitrogen atoms and formation of carbon monoxide, carbon dioxide, and nitrogen oxides or other volatile components, which was responsible for the mass loss of the hybrid films. The Si 2p peak deconvolution results of 29.7 wt % HBPSi polyimide before and after exposure to a variety of AO fluences at different binding energies are shown in Table 4. Before AO exposure,

Table 4. Peak Deconvolution Results of Si 2p for 29.7 wt % HBPSi Polyimide at Different Binding Energies Determined from XPS Spectra

	area fraction (%)		
exposure duration (h)	100.8 eV (Si−C)	102 eV ($RSiO_{1.5}$)	103.6 eV (SiO_2)
0	0.9	98.9	0.2
5	0.7	1.5	97.8
10	0.3	1.0	98.7
15		0.9	99.1
22			100

most of the silicon atoms were present at low binding energy (102 eV), approximately $RSiO_{1.5}$ (still in the form of polysiloxane). However, 97.8% of surface Si atoms formed SiO_2 after 5 h AO exposure, indicating that hyperbranched polysiloxane was much more effective in formation of SiO_2 layer. Furthermore, after 22 h exposure, almost all Si atoms of the topmost surface converted to SiO_2. Likewise, as can be seen in Table 3, both carbon and nitrogen atom concentrations reached their minimum value, suggesting that chemical bonds of C−C and C−N in benzene and imide rings are predominantly broken by AO irradiation. Thereby the surface components of 29.7 wt % HBPSi polyimide were mainly inorganic SiO_2. Upon AO exposure, the silicon had reacted with AO, thus the binding energy of inner electrons had increased, and the oxidation state of the silicon essentially converted into a passivation layer in the form of SiO_2,[26,27,36,59] which was further evidenced by the high-resolution XPS spectra of Si 2p and O 1s curves, seen in Figure 11b,c. The peaks in the Si 2p and O 1s spectra exhibited evident shifts of 1.6 and 0.9 eV, respectively, again testifying that the silicon near the film surface was oxidized approximately to SiO_2.[26]

3.5. Discussion of Protection and Erosion Mechanism of HBPSi Polyimide. As discussed above, oxidation effects might account for the mass loss and the decrease in carbon atom concentrations. However, after 22 h exposure, as shown in Table 3, the entire organic polyimide moiety of the topmost surface had almost been etched at the early stage by the incoming AO. This is to say that only inorganic silica was left on the surface of the hybrid polyimide, which was not sensitive to AO and protected the underlying polymer from further degradation. Nevertheless, as an earlier investigation reported,[27] apparent mass losses could still be detected albeit silicon-containing polyimides suffered fairly long duration AO exposure. Their mass loss rates decreased with exposure fluence and appeared to tend toward but did not go to zero or reach a constant low value.[27] This phenomenon indicated the

SiO_2 passivation layer was not so perfect or defect-free or was never completely impervious to AO as we originally expected. In other words, it could not completely prevent the AO attack. In order to elucidate this phenomenon, the surfaces of 29.7 wt % HBPSi polyimide after exposure to different AO fluences were observed by SEM in high magnification mode, as shown in Figure 12. As indicated, a certain amount of pinholes and

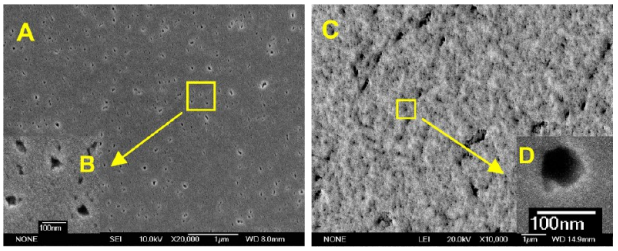

Figure 12. SEM images of 29.7 wt % HBPSi polyimide exposed to AO for 10 h (A, B) and 22 h (C, D).

microcracks with diameters of about 20−60 nm appeared on the exposed film surfaces. It is these defects that possibly play the role of the channels or pathways for the AO to diffuse into the bulk polymer and eventually etch the organic polymers underneath this passivation layer, eventually leading to the mass loss of HBPSi polyimide during long duration AO exposure. The formation of these pinholes and microcracks was presumably ascribed to the following reasons. First, the SiO_2 passivation layer was so brittle that once the thickness of this layer exceeded a certain critical value, rupture could possibly appear. Besides, the formation of SiO_2 layer probably led to internal stresses because of a volume (or density) change or due to the mismatch of the coefficient of thermal expansion (CTE) between the substrate polymer and the SiO_2 layer. Furthermore, the internal stresses might induce coating spalling, delaminating, cracking, or disbanding, which were also possible sources of the defects. As Table 3 shows, the nitrogen atom concentration, which was considered as the characteristic chemical component of polyimide, changed irregularly with increasing AO fluence, in agreement with the earlier reports.[26] Thus it would make sense that the formation or regrowth and breakage of the SiO_2 protective layer were likely to be a dynamic equilibrium. Despite the minor defects forming on the film surfaces, the HBPSi polyimide still exhibited desirable anti-AO erosion properties. Moreover, HBPSi was incorporated into polyimide chains and dispersed uniformly in the polymer matrix. Thus, once the passivation layer was spalled or disbanded, the underlying polymer was again exposed to AO and was eroded at the early stage, and finally the protective layer could again be established, inhibiting the underlying polymer from further erosion, which enabled the hybrid polyimide surface to be "self-healing". Based on the above analysis, the protection and erosion mechanism of HBPSi polyimide can be described as follows. Upon AO exposure, the polyimide on the topmost surface might be first degraded while silicon atoms remained and reacted with AO and gradually oxidized approximately to SiO_2. It was this passivation SiO_2 layer on the surface of HBPSi polyimide that protected the underlying polymer from additional erosion. This protective layer was not completely defect-free or never impervious to AO attack, which led to the mass loss of hybrid films during long duration AO exposure. The breakage and regrowth of the protective layer were constantly emerging during the whole exposure period. The mechanism could be depicted as in Figure 13.

3.6. Optical Transparency of the Prepared Polyimide Thin Films before and after Exposure to AO. In a practical application, polyimide films are used extensively onboard spacecraft, mainly as thermal blankets, space inflatable structure membrane materials, critical components in solar arrays and thermal control materials on the long duration exposure facility (LDEF).[1,9,59,60] However, two of several important properties of polyimides for space applications are α and ε.[16] Solar absorptivity (α) refers to the fraction of incoming solar energy absorbed by the film, and ε is an evaluation of the film's thermal emission ability. Typically, a light-colored and highly transparent film exhibits low α value.[16] In many applications, it is desired to have this ratio of α/ε less than 0.5 over the lifespan of the materials.[5] Polymers that exhibit significant change in the α/ε ratio are less efficient in their ability to maintain the thermal stability of spacecraft. Thus in order to reduce the α/ε ratio, solar absorption of polyimide films, that is, the α value, should be lowered as far as possible. For this reason, transparency should be improved and charge transfer complexes (CTC) should be disrupted to prepare light-colored polyimide films, ensuring polyimide films could be widely used as critical components in solar arrays or inflatable structure membrane materials or thermal control materials on spacecrafts.

HBPSi contains a three-dimensional compact structure and thus provides evident steric hindrance and a highly irregular structure to the molecule skeleton of polyimide. This was expected to disrupt the formation of CTC and lead to light-colored polyimide films with high optical transparency.[16] As

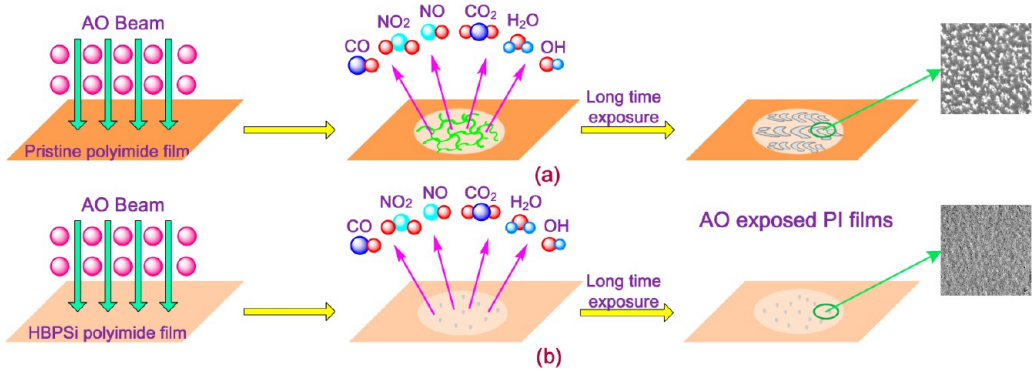

Figure 13. Schematic diagram of the erosion and protective mechanism of (a) pristine and (b) HBPSi polyimide films during AO exposure.

shown in Figure 14, a photograph of a lotus flower could be clearly observed through 29.7 wt % HBPSi polyimide film,

Figure 14. Photograph of HBPSi-PI over a photograph of a lotus flower (right).

indicating HBPSi polyimide film possesses desirable transparency. Thin films were measured for optical transparency with the percent transmission at 600 nm illustrated in Table 2. All the polyimide films exhibited optical transparency above 75%. However, as can be seen in Table 3 and Figure 15, the pristine polyimide turned somewhat opaque and the optical transparency at 600 nm remarkably decreased with increasing exposure fluence. After 22 h exposure, the transmittance was merely 18%. This was probably owing to the extremely rough film surfaces, increasing light absorption and surface scattering loss.[55] On the contrary, the transmittance of 29.7 wt % HBPSi polyimide slightly decreased; after 15 h exposure, the optical transparency was still as high as 72%. The excellent optical transparency with HBPSi polyimides demonstrated great promise for HBPSi polyimides as candidates for the wide use as optoelectronic devices, space inflatable structure membrane materials, critical components in solar arrays, thermal control materials on spacecrafts, or on the long duration exposure facility (LDEF).

4. CONCLUSIONS

Polysiloxane with highly hyperbranched topology and high silicon content was successfully synthesized, characterized, and subsequently reacted with ODA and PMDA to prepare a novel space-survivable HBPSi polyimide for the first time. The whole preparation process was moderate, low-cost, environmentally friendly, and suitable for industrialized mass production. The resulting polyimides exhibited a combination of desirable properties such as excellent thermal stability, high optical transparency, good mechanical strength, satisfactory break elongation, and outstanding anti-AO erosion properties. During HBPSi polyimide exposure to AO, the organic polyimide of the topmost surface was degraded at the early stage and a silica passivation layer was formed, which was confirmed by XPS core level spectra of C 1s, Si 2p, and O 1s. This SiO_2 layer grew with exposure duration or AO fluence and became increasingly resistant to atomic oxygen attack. It was found that the erosion yield of these hybrid polyimides decreased with increasing the HBPSi addition and AO fluence. The incorporation of HBPSi into the polyimide backbone was not only responsible for endowing polyimide with outstanding AO resistance but also responsible for the high optical transparency of HBPSi polyimide after long duration AO exposure. As the AO fluence increased to 3.87×10^{20} O atoms·cm^{-2}, the 29.7 wt % HBPSi polyimide exhibited less rough surface morphology than the pristine polyimide film and the AO erosion yield reached as low as 7.97% that of standard Kapton H. The presence of a certain amount of pinholes and microcracks possibly accounted for the apparent mass loss of HBPSi polyimide after exposure with fairly high AO fluence. The formation or regrowth and breakage of the SiO_2 protective layer were likely to be a dynamic equilibrium, and this phenomenon was constantly emerging during the whole exposure period. The increase in the AO resistance property of HBPSi polyimide film was the consequence of the formation of passivation SiO_2 layer. This SiO_2 protective layer enables the surface to be "self-healing" and is desirable for HBPSi polyimide as a "drop-in" replacement for the widely used Kapton on spacecrafts functioning in space environment.

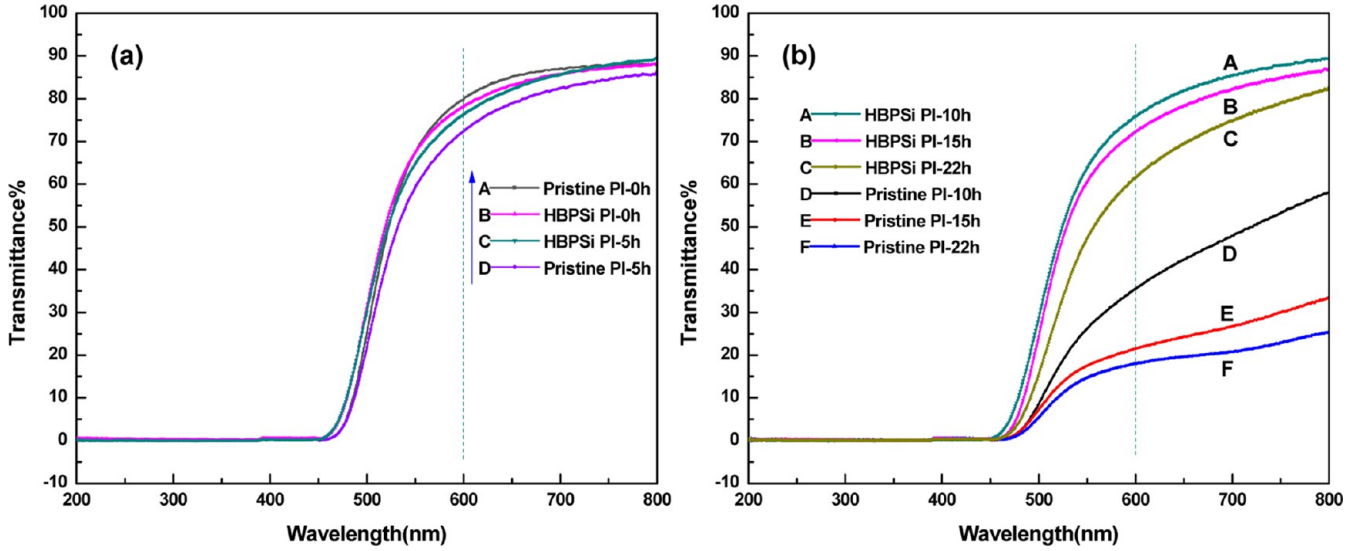

Figure 15. Transmission spectra of pristine polyimide and 29.7 wt % HBPSi polyimide before and after exposure to a variety of AO fluences of (a) 0.88×10^{20} O atoms·cm^{-2} (5 h); (b) 1.76×10^{20} O atoms·cm^{-2} (10 h), 2.64×10^{20} O atoms·cm^{-2} (15 h), and 3.87×10^{20} O atoms·cm^{-2} (22 h), respectively.

5. PROSPECT

Hitherto, considerable progress has been achieved in terms of development of new materials that can withstand the space hazards and the protective enhancement mechanism of these novel polyimides is generally recognized as first degradation of organic portions and eventually in situ buildup of a passivation layer, such as SiO_2, polyphosphate, or other AO-insensitive substances on the top surface of polyimide upon long duration AO exposure. However, whether this passivation layer never becomes completely impervious to AO or not still remains undefined. Additionally, the problem of what kind of protective layer, SiO_2 or polyphosphate or other passivation layer, is the most effective to protect the underlying polymers from AO erosion is still not settled yet. Thus, the above two aspects should be the focus of the future work.

AUTHOR INFORMATION

Corresponding Author

*E-mail: qyzhang@nwpu.edu.cn; Tel: +86-029-88431675; Fax: +86-029-88431653.

Notes

The authors declare no competing financial interest.

ACKNOWLEDGMENTS

The authors are grateful for the financial support provided by the National Natural Science Foundation of China (Grant Nos. 51173146 and 51173147), Basic Research Fund of Northwestern Polytechnical University (Grant JC20120248), Key Project of Space Foundation (Grant CASC201106), and Graduate Starting Seed Fund of Northwestern Polytechnical University (Grant No. Z2013163).

REFERENCES

(1) Dever, J. A.; Miller, S. K.; Sechkar, E. A.; Wittberg, T. N. *High Perform. Polym.* **2008**, *20*, 371−387.

(2) Zhao, X. H.; Shen, Z. G.; Xing, Y. S.; Ma, S. L. *J. Phys. D: Appl. Phys.* **2001**, *34*, 2308−2314.

(3) Reddy, M. R. *J. Mater. Sci.* **1995**, *30*, 281−307.

(4) Waters, D. L.; Banks, B. A.; De Groh, K. K.; Miller, S. K. R.; Thorson, S. D. *High Perform. Polym.* **2008**, *20*, 512−522.

(5) Schuler, P.; Mojazza, H. B.; Haghighat, R. *High Perform. Polym.* **2000**, *12*, 113−123.

(6) Schuler, P.; Haghighat, R.; Mojazza, H. *High Perform. Polym.* **1999**, *11*, 113−121.

(7) Skurat, V. E.; Samsonov, P. V.; Nikiforov, A. P. *High Perform. Polym.* **2004**, *16*, 339−355.

(8) Nicholson, K. T.; Sibener, S. J.; Minton, T. K. *High Perform. Polym.* **2004**, *16*, 197−206.

(9) De Groh, K. K.; Banks, B. A.; Mccarthy, C. E.; Rucker, R. N.; Roberts, L. M.; Berger, L. A. *High Perform. Polym.* **2008**, *20*, 388−409.

(10) Buczala, D. M.; Brunsvold, A. L.; Minton, T. K. *J. Spacecr. Rockets* **2006**, *43*, 421−425.

(11) Koontz, S. L.; Albyn, K.; Leger, L. J. *J. Spacecr. Rockets* **1991**, *28*, 315−323.

(12) Fong, H.; Vaia, R. A.; Sanders, J. H.; Lincoln, D.; Vreugdenhil, A. J.; Liu, W. D.; Bultman, J.; Chen, C. G. *Chem. Mater.* **2001**, *3*, 4123−4129.

(13) Murad, E. *J. Spacecr. Rockets* **1996**, *33*, 131−136.

(14) Connell, J. W.; Smith Jrt, J. G.; Hergenrother, P. M. *Polymer* **1995**, *36*, 5−11.

(15) Connell, J. W.; Smith, J. G., Jr. *Polymer* **1995**, *36*, 13−19.

(16) Watson, K. A.; Palmieri, F. L.; Connell, J. W. *Macromolecules* **2002**, *35*, 4968−4974.

(17) Peters, W. C; Harris, G.; Miller, G.; Petro, J. *High Perform. Polym.* **2000**, *12*, 105−112.

(18) Gouzman, I.; Girshevitz, O.; Grossman, E.; Eliaz, N.; Sukenik, C. N. *ACS Appl. Mater. Interfaces* **2010**, *2*, 1835−1843.

(19) Minton, T. K.; Wu, B. H.; Zhang, J. M.; Lindholm, N. F.; Abdulagatov, A. I.; O'Patchen, J.; George, S. M.; Groner, M. D. *ACS Appl. Mater. Interfaces* **2010**, *2*, 2515−2520.

(20) Gouzman, I.; Grossman, E.; Lempert, G.; Noter, Y.; Altshuler, Y.; Lifshitz, Y. *High Perform. Polym.* **2001**, *13*, S505−S516.

(21) Tagawa, M.; Yokota, K.; Kishida, K.; Okamoto, A.; Ishizawa, J.; Minton, T. K. *High Perform. Polym.* **2010**, *22*, 213−224.

(22) Brunsvold, A. L.; Zhang, J. M.; Upadhyaya, H. P.; Minton, T. K. *ACS Appl. Mater. Interfaces* **2009**, *1*, 187−196.

(23) Zhang, J. M.; Lindholm, N. F.; Brunsvold, A. L.; Upadhyaya, H. P.; Minton, T. K. *ACS Appl. Mater. Interfaces* **2009**, *1*, 653−660.

(24) Yokota, K.; Ohmae, N.; Tagawa, M. *High Perform. Polym.* **2004**, *16*, 221−234.

(25) Verker, R.; Grossman, E.; Eliaz, N. *Acta Mater.* **2009**, *57*, 1112−1119.

(26) Brunsvold, A. L.; Minton, T. K.; Gouzman, I.; Grossman, E.; Gonzalez, R. *High Perform. Polym.* **2004**, *16*, 303−318.

(27) Minton, T. K.; Wright, M. E.; Tomczak, S. J.; Marquez, S. A.; Shen, L. H.; Brunsvold, A. L.; Cooper, R.; Zhang, J. M.; Vij, V.; Guenthner, A. J.; Petteys, B. J. *ACS Appl. Mater. Interfaces* **2012**, *4*, 492−502.

(28) Xiao, F.; Wang, K.; Zhan, M. S. *J. Mater. Sci.* **2012**, *47*, 4904−4913.

(29) Devapal, D.; Packirisamy, S.; Reghunadhan Nair, C. P.; Ninan, K. N. *J. Mater. Sci.* **2006**, *41*, 5764−5766.

(30) Köytepe, S.; Paşahan, A.; Ekinci, E.; Alıcı, B.; Seçkin, T. *J. Polym. Res.* **2008**, *15*, 249−257.

(31) Thompson, C. M.; Smith, J. G.; Connell, J. W. *High Perform. Polym.* **2003**, *15*, 181−195.

(32) Connell, J. W. *High Perform. Polym.* **2000**, *12*, 43−52.

(33) Zhang, X. W.; Ren, H. Y.; Wang, J. H.; Zhang, Y.; Shao, Y. Y. *Mater. Lett.* **2011**, *65*, 821−824.

(34) Gonzalez, R. I.; Phillips, S. H. *J. Spacecr. Rockets* **2000**, *37*, 463−467.

(35) Devapal, D.; Packirisamy, S.; Korulla, R. M.; Ninan, K. N. *J. Appl. Polym. Sci.* **2004**, *94*, 2368−2375.

(36) Yokota, K.; Abe, S.; Tagawa, M.; Iwata, M.; Miyazaki, E.; Ishizawa, J. I.; Kimoto, Y.; Yokota, R. *High Perform. Polym.* **2010**, *22*, 237−251.

(37) Wright, M. E.; Schorzman, D. A.; Feher, F. J.; Jin, R. Z. *Chem. Mater.* **2003**, *15*, 264−268.

(38) Tomczak, S. J.; Wright, M. E.; Guenthner, A. J.; Petteys, B. J.; Brunsvold, A. L.; Knight, C.; Minton, T. K.; Vij, V.; McGrath, L. M.; Mabry, J. M. Space Survivability of Main-Chain and Side-Chain POSS-Kapton Polyimides. In *AIP Conference Proceedings: Materials Physics and Applications*; Kleiman, J. I, Ed.; Springer: New York, 2009; Vol. *1087*, pp 505−518.

(39) Tomczak, S. J.; Wright, M. E.; Guenthner, A. J.; Petteys, B. J.; Minton, T. K.; Brunsvold, A.; Vij, V.; McGrath, L. M.; Mabry, J. M. The Effect of Atomic Oxygen on POSS Polyimides. *SAMPE Conference Proceedings 2008*; Society for the Advancement of Materials and Process Engineering: Covina, CA, 2008; Vol. *53*, pp 306/1−306/15.

(40) Ye, J. H.; Liang, G. Z.; Gu, A. J.; Zhang, Z. Y.; Han, J. P.; Yuan, L. *Polym. Degrad. Stab.* **2013**, *98*, 597−608.

(41) Nair, B. P.; Pavithran, C. *Langmuir* **2010**, *26*, 730−735.

(42) Huang, J. C.; He, C. B.; Xiao, Y.; Mya, K. Y.; Dai, J.; Siow, Y. P. *Polymer* **2003**, *44*, 4491−4499.

(43) Young, S. K.; Jarrett, W. L.; Mauritz, K. A. *Polymer* **2002**, *43*, 2311−2320.

(44) Peeters, M. P. J.; Wakelkamp, W. J. J.; Kentgens, A. P. M. *J. Non-Cryst. Solids* **1995**, *189*, 77−89.

(45) Alam, T. M.; Assink, R. A.; Loy, D. A. *Chem. Mater.* **1996**, *8*, 2366−2374.

(46) Babonneau, F.; Thorne, K.; Mackenzie, J. D. *Chem. Mater.* **1989**, *1*, 554−558.

(47) Holter, D.; Frey, H. *Acta Polym.* **1997**, *48*, 298−309.

(48) Hawker, C. J.; Lee, R.; Fréchet, J. M. J. *J. Am. Chem. Soc.* **1991**, *113*, 4583−4595.
(49) Chen, H.; Kong, J.; Tian, W.; Fan, X. D. *Macromolecules* **2012**, *45*, 6185−6195.
(50) Satoh, T.; Tamaki, M.; Taguchi, T.; Misaka, H.; Hoai, N. T.; Sakai, R.; Kakuchi, T. *J. Polym. Sci., Part A: Polym. Chem.* **2011**, *49*, 2353−2365.
(51) Wang, S. J.; Fan, X. D.; Kong, J.; Wang, X.; Liu, Y. Y.; Zhang, G. B. *J. Polym. Sci., Part A: Polym. Chem.* **2008**, *46*, 2708−2720.
(52) Kong, J.; Schmalz, T.; Motz, G.; Müller, A. H. E. *Macromolecules* **2011**, *44*, 1280−1291.
(53) Tian, W.; Fan, X. D.; Kong, J.; Liu, T.; Liu, Y. Y.; Huang, Y.; Wang, S. J.; Zhang, G. B. *Macromolecules* **2009**, *42*, 640−651.
(54) Mori, H.; Müller, A. H. E.; Simon, P. F. W. In *Macromolecular Engineering: Precise Synthesis, Materials, Properties, Applications*; Matyjaszewski, K., Gnanou, Y., Leibler, L., Eds.; Wiley-VCH: Weinheim, Germany, 2007; Vol. 2, p 973.
(55) Chang, C. C.; Chen, W. C. *Chem. Mater.* **2002**, *14*, 4242−4248.
(56) Liu, Y. L.; Liu, C. S.; Cho, C. I.; Hwu, M. J. *Nanotechnology* **2007**, *18*, 225701−225705.
(57) Leu, C. M.; Chang, Y. T.; Wei, K. H. *Macromolecules* **2003**, *36*, 9122−9127.
(58) Kinoshita, H.; Tagawa, M.; Yokota, K.; Ohmae, N. *High Perform. Polym.* **2001**, *13*, 225−234.
(59) Verker, R.; Grossman, E.; Gouzman, I.; Eliaz, N. *High Perform. Polym.* **2008**, *20*, 475−491.
(60) Silverman, E. M. Space Environmental Effects on Spacecraft−LEO Material Selection Guide. NASA Contractor Report No. 4661. Langley Research Center, 1995, Part 1−2.